



Cite this: *Biomater. Sci.*, 2019, **7**, 4099

Dual bioresponsive antibiotic and quorum sensing inhibitor combination nanoparticles for treatment of *Pseudomonas aeruginosa* biofilms *in vitro* and *ex vivo*[†]

Nishant Singh,^{‡a} Manuel Romero,^{‡b} Alessandra Travanut,^a Patricia F. Monteiro,^{ib a} Elena Jordana-Lluch,^{ib c} Kim R. Hardie,^{ib c} Paul Williams,^{ib c} Morgan R. Alexander^{ib a} and Cameron Alexander^{ib *a}

Many debilitating infections result from persistent microbial biofilms that do not respond to conventional antibiotic regimens. A potential method to treat such chronic infections is to combine agents which interfere with bacterial biofilm development together with an antibiotic in a single formulation. Here, we explore the use of a new bioresponsive polymer formulation derived from specifically modified alginate nanoparticles (NPs) in order to deliver ciprofloxacin (CIP) in combination with the quorum sensing inhibitor (QSI) 3-amino-7-chloro-2-nonylquinazolin-4(3H)-one (ACNQ) to mature *Pseudomonas aeruginosa* biofilms. The alginate NPs were engineered to incorporate a pH-responsive linker between the polysaccharide backbone and the QSI, and to encapsulate CIP via charge–charge interactions of the positively-charged drug with the carboxyl residues of the alginate matrix. In this way, a dual-action release of antibiotic and QSI was designed for the low-pH regions of a biofilm, involving cleavage of the QSI-linker to the alginate matrix and reduced charge–charge interactions between CIP and the polysaccharide as the alginate carboxyl side-chains protonated. When tested in a biofilm model the concomitant release of CIP + QSI from the pH-responsive nanoparticles significantly reduced the viability of the biofilm compared with CIP treatment alone. In addition, the alginate NPs were shown to penetrate deeply into *P. aeruginosa* biofilms, which we attribute in part to the charges of the NPs and the release of the QSI agent. Finally, we tested the formulation in both a 2D keratinocyte and a 3D *ex vivo* skin infection model. The dual-action bio-responsive QSI and CIP release nanoparticles effectively cleared the infection in the latter, suggesting considerable promise for combination therapeutics which prevent biofilm formation as well as effectively killing mature *P. aeruginosa* biofilms.

Received 18th May 2019,

Accepted 1st July 2019

DOI: 10.1039/c9bm00773c

rs.c.li/biomaterials-science

Introduction

The increasing problems of multi-antibiotic resistance urgently require alternative therapeutic options.^{1–3} One of the

main issues associated with indiscriminate antibiotic use is the activation of defence mechanisms in pathogens,⁴ and as a survival strategy, bacteria form biofilms.⁵ These are surface-associated multicellular communities embedded in a self-generated extracellular matrix (ECM).⁶ The latter is composed of polysaccharides, proteins and extracellular DNA (eDNA), and is both heterogeneous in composition and architecture, as well as resistant to penetration by antimicrobial agents.⁷ Upon administration, most antibiotics kill the more susceptible planktonic bacterial cells, leaving behind the intrinsically antibiotic tolerant biofilm embedded bacteria. The tolerance of biofilms to antimicrobial agents generally is multifactorial involving physical, physiological and intrinsic genetic determinants whereas antibiotic resistance is a consequence of mutations and the acquisition of antibiotic resistance genes *via* horizontal gene transfer.⁸ Biofilms are also refractory to clearance by the host immune system and so elicit a number

^aSchool of Pharmacy, University of Nottingham, University Park, Nottingham NG7 2RD, UK. E-mail: cameron.alexander@nottingham.ac.uk

^bNational Biofilms Innovation Centre (NBIC), School of Life Sciences, University of Nottingham, Centre for Biomolecular Sciences, University Park, NG7 2RD, UK

^cSchool of Life Sciences, University of Nottingham, Centre for Biomolecular Sciences, University Park, NG7 2RD, UK

[†]Electronic supplementary information (ESI) available. See DOI: 10.1039/c9bm00773c

[‡]These authors contributed equally to this work.

[§]Current affiliation: Antibiotic Resistance and Pathogenicity of Bacterial Infections Group, Balearic Islands Health Research Institute (IdISBa), 07120, Palma, Spain.



of major clinical challenges, such as chronic inflammation, impaired wound healing and systemic spread of chronic infections.⁹ Novel therapeutic strategies are thus urgently needed to combat the threat of biofilm-centred infections.^{10–17}

One of the most promising approaches is the combined-use of antibiotics with adjuvants that do not affect the pathways essential for the bacterial growth and viability, and as a consequence are less likely to select for resistance. Such agents have various modes of action including (i) increasing bacterial cell membrane permeability, (ii) impairing biofilm formation, and/or the production of virulence factors and antibiotic resistance elements, (iii) blocking antibiotic efflux pumps and (iv) changing phenotype from the biofilm to the planktonic state through biofilm dispersal. Since bacterial communities co-ordinate their pathogenic activities including biofilm development through cell–cell communication (quorum sensing, QS)^{5,18} using small diffusible signal molecules, disruption of QS interferes with biofilm formation and maturation.^{19–23} However, while there are combination formulations in the clinic which use antibiotics and β -lactamase inhibitors (e.g. Tazocin®, Unasyn® Augmentin®), none to date have utilised QS inhibitors (QSIs) as biofilm disrupting agents. Several QS and QSI control and release systems have however been described, including molecularly imprinted polymers which bind the QS agents to suppress bacterial biofilm formation, and peptide mimetics which disrupt biofilms of several bacterial strains.^{24–29}

Here we set out to prepare a new antimicrobial biofilm formulation which would have the following attributes, (i) QS inhibition, (ii) broad spectrum antibiotic activity, (iii) good biofilm penetration, and (iv) good tissue compatibility with low cytotoxicity. We selected the clinically important bacterium *Pseudomonas aeruginosa* as the model organism, as this pathogen is responsible for more than 30% of hospital-acquired infections and causes chronic biofilm-centred infections in diverse body sites. This organism is also intrinsically resistant to many antibiotics and a member of the ESKAPE group of multi-antibiotic resistant bacterial pathogens.³⁰ For the QS inhibitor (QSI), we selected 3-amino-7-chloro-2-nonylquinazolin-4(3*H*)-one (ACNQ), a potent inhibitor of the pseudomonas quinolone QS system which targets the PqsR receptor. ACNQ inhibits virulence factor production and biofilm development and in particular reduces the production of matrix components including eDNA and rhamnolipids.³¹ The second component was ciprofloxacin, (CIP), a fluoroquinolone antibiotic with broad spectrum activity but also a drug to which bacterial pathogens including *P. aeruginosa* have acquired resistance.³² In order to penetrate a dense biofilm matrix, we chose to encapsulate the antibiotic and conjugate the QSI within *in situ*-formed sodium alginate nanoparticles. These carry a net negative charge at the pH values likely to be encountered in many bacterial biofilms. In addition, alginate oligosaccharides have been reported to disrupt biofilm formation and maturation and potentiate antibiotic action against *P. aeruginosa*.³³ We thus anticipated that the alginate nanoparticles might penetrate further into the biofilm since

the ECM contains polyanion-containing exopolysaccharides and eDNA³⁴ as well as the negatively charged *P. aeruginosa* cell envelope,³⁵ compared with ACNQ (weakly basic) and CIP (zwitterionic, but with a net positive charge at pH 7.4). In addition, alginates are already widely used in oral formulations, have a proven safety profile, are readily available, and can be derivatised further due to their multiple carboxyl residues.³⁶

The combined formulation thus consisted of alginate-based nanoparticles (NPs), containing CIP encapsulated by charge–charge interactions during a nanoprecipitation process, with ACNQ attached *via* a pH-responsive hydrazine linker, and of a size range (150–200 nm) similar to those of *Pseudomonas* bacteriophages.³⁷ We then tested these formulations as synergistic adjuvant-drug therapeutics in infection models consisting of pre-established biofilms of *P. aeruginosa* PAO1-Nottingham subline (PAO1-N) of $\geq 100\ \mu\text{m}$ thickness *in vitro* and in both 2D and 3D skin infection models. The formulation and anti-infective action is shown schematically in Fig. 1.

Materials and methods

Experimental

Materials. 2-Ethynylbenzaldehyde, 2-chloro-4,6-dimethoxy-1,3,5-triazine (CDMT), and trimethylamine (TEA) were purchased from Acros Organics. 4-Methylmorpholine (NMM), 6-amino fluorescein, ciprofloxacin, 11-azido-3,6,9-trioxadecan-1-amine, blue fluorescent polystyrene-NH₂ nanoparticles ($\lambda_{\text{ex}} \sim 360\ \text{nm}$; $\lambda_{\text{em}} \sim 420\ \text{nm}$, *d*-50 nm), and deuterated chloroform (CDCl₃), water (D₂O), and dimethyl sulfoxide (DMSO-D₆) were purchased from Sigma-Aldrich. Pronova UPVLVG Alginate was bought from Novamatrix. Dialysis tubes (10 000 Da, 3500 Da and 2000 Da MWCO) and Red fluorescent polystyrene-NH₂ nanoparticles ($\lambda_{\text{ex}} \sim 580\ \text{nm}$; $\lambda_{\text{em}} \sim 605\ \text{nm}$, *d*-200 nm) were purchased from ThermoFisher Scientific. All other analytical and synthesis grade solvents were purchased from ThermoFisher Scientific.

Instrumentation. ¹H and ¹³C NMR spectra were obtained using a Bruker DPX400 UltraShieldTM spectrometer at 400 MHz (¹H and ¹³C). An AV(III) 500 NMR spectrometer with carbon–hydrogen Cryoprobe at 500 MHz was used to acquire ¹³C NMR of the polymers ALG_{ALD} and ALG_{QSI}. The FTIR spectra of the lyophilized alginate polymer samples (N₃-PEG₃-ALG, ALG_{ALD} and ALG_{QSI}) were obtained using 64 scans with CARY 630 FTIR spectroscopic suite by Agilent Technologies. Nanoparticle morphology was analysed using a Tecnai G2 (FEI, Oregon USA) transmission electron microscope (TEM). The size and zeta potential of NPs were measured at 25 °C by dynamic light scattering (DLS, Zetasizer Nano ZS90, Malvern Instruments Ltd, UK). Drug encapsulation and release experiments were quantified using a Cary 50 Bio UV spectrometer. Confocal laser scanning microscopy was carried out using a LSM 700 microscope (Carl Zeiss, Germany) and 96-well plates were imaged using TECAN Genios Pro reader (Tecan, UK).



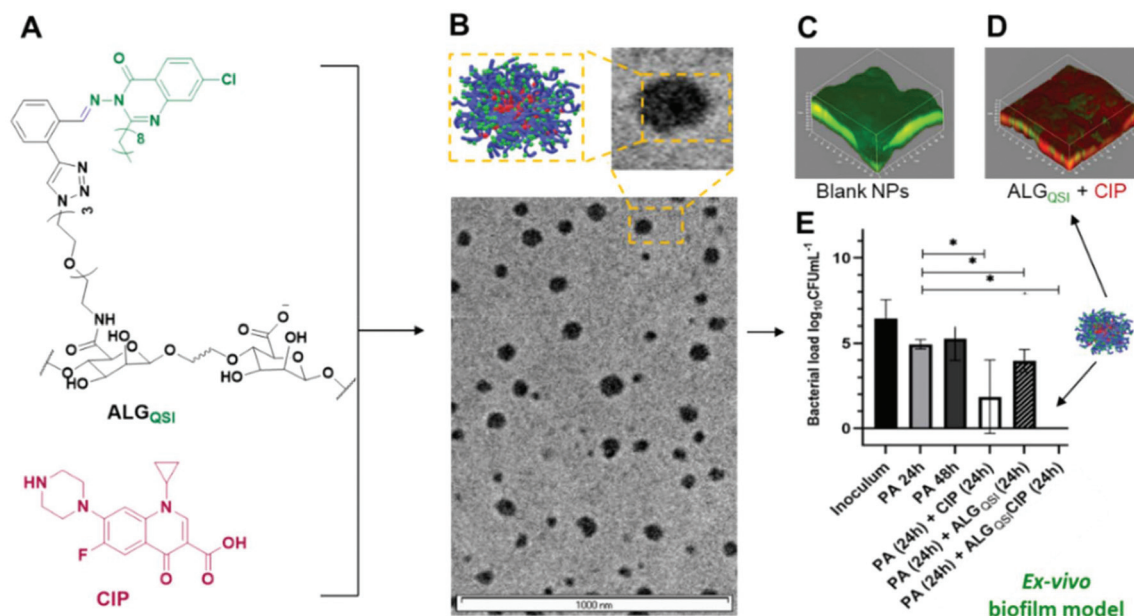


Fig. 1 Schematic of combined polymer, QSI and antibiotic nanoparticle formulation (A, B) and activity against *P. aeruginosa* biofilms *in vitro* (C, D, E). Structures of components are shown in (A) with TEM micrographs in (B). In (C) viable *P. aeruginosa* are labelled green following treatment with blank NPs; while in (D) non-viable cells are labelled red following incubation with ALG_{QSI} + CIP. Efficacy in an *ex vivo* infected skin model is shown in (E).

Synthesis

(Z)-7-Chloro-3-((2-ethynylbenzylidene)amino)-2-nonylquinazolin-4(3H)-one. To a solution of 2-ethynylbenzaldehyde (50 mg, 4 equiv., 0.384 mmol) and triethylamine (100 μ L) in dry methanol (20 mL), was added ACNQ, synthesized as described before³¹ (30 mg, 1 equiv., 0.096 mmol) under an argon atmosphere and the mixture was stirred at 50 $^{\circ}$ C for 72 h. Methanol was then evaporated under vacuum. The obtained reaction mixture was purified by column chromatography to obtain the pure product as an off-white solid in 80% yield (eluent: MeOH/triethylamine/ CHCl_3 -4/1/95). ESI-predicted mass – 433.19, Mass found+ H^+ -434.2006.

^1H NMR (CDCl_3 , 400 MHz, 25 $^{\circ}$ C), δ (ppm) 1H (9.55, s), 2H (8.26–8.24, d), 1H (7.72–7.73, d), 1H (7.67–7.62, dd), 2H (7.60–7.50, p), 1H (7.44–7.41, dd), 1H (3.43, s), 2H (2.98–2.94, t), 2H (1.86–1.79, p), 2H (1.59, s), 2H (1.45–1.40, s), 8H (1.40–1.25, m), 3H (0.90–0.57, t). ^{13}C NMR (101 MHz, CDCl_3) δ 165.1, 158.24, 158.2, 147.4, 140.4, 134.3, 133.4, 131.9, 129.2, 128.8, 126.9, 126.7, 126.1, 124.4, 119.9, 84.0, 79.9, 35.2, 31.8, 29.4, 29.3, 29.3, 29.2, 26.7, 22.6, 14.1.

11-Azido-3,6,9-trioxaundecanamido-alginate (N_3 -TEG-ALG). Sodium alginate (1 equiv., 400 mg = 2.08 mmol of $-\text{COOH}$) was dissolved as a 2% alginate solution in a 12 mL : 8 mL – water : acetonitrile mixture at 55 $^{\circ}$ C. 11-Azido-3,6,9-trioxaundecan-1-amine (1 equiv., 2.08 mmol, 453 mg) was then added to the mixture along with the coupling reagents 2-chloro-4,6-dimethoxy-1,3,5-triazine (CDMT, 0.5 equiv., 1.04 mmol, 180 mg) and 4-methylmorpholine (NMM, 1 equiv., 2.08 mmol, 224 μ L). The mixture was stirred at 55 $^{\circ}$ C for 16 h after which

the solvent was removed under reduced pressure. The resulting solid was dissolved in water and filtered through cyano-modified silica gel to remove insoluble precipitates. The obtained solution was then dialyzed against a 10 000 MWCO dialysis membrane for 2 days with DI water. The solution was then lyophilized to obtain the purified polymer. ^1H NMR (D_2O , 400 MHz, 25 $^{\circ}$ C), δ (ppm)-6.57 (s, Alg-CO-NH- CH_2CH_2 -(OCH_2CH_2) $_3$ - N_3), 5.10–4.90 (m, alginate), 4.60–3.80 (alginate, m), 3.80–3.50 (-(OCH_2CH_2) $_3$ -O, 12H, m), 3.50–3.35 (Alg-CO-NH- CH_2CH_2 -O-, 2H, t), 3.20–3.10 (-(OCH_2CH_2 - N_3 , 2H, t). IR (wavenumber, cm^{-1}) – 1600 (CO-NH amide stretch), 2100 (N_3 (azide) stretch), 2879, 2918 (CH stretch), 3278 ($-\text{COOH}$ stretch).

Aldehyde-functional alginate and QSI-alginate conjugate (ALG_{ALD} or ALG_{QSI}). 11-Azido-3,6,9-trioxaundecanamido-alginate (N_3 -TEG-ALG, 100 mg) was dissolved in a solution of water : methanol 1 : 1 (5 mL) at 55 $^{\circ}$ C. To this solution were added tris[1-benzyl 1H-1,2,3-triazol-4-yl] methylamine (TBTA, 0.2 equiv., 50 mg), triethylamine (0.25 equiv., typically 15 μ L), and copper(I)-iodide (0.25 equiv., 5 mg) as coupling agents. Then 0.51 mmol of 2-ethynylbenzaldehyde (for ALG_{ALD}) or (Z)-7-chloro-3-((2-ethynylbenzylidene)amino)-2-nonylquinazolin-4(3H)-one (for ALG_{QSI}) was added and the mixture was stirred at 55 $^{\circ}$ C overnight. The solvent was removed under reduced pressure and the oily product was resuspended in 5 mL of water and dialyzed. The resulting solution was then dialyzed using a 10 000 MWCO dialysis membrane in phosphate buffer pH 7.4 to purify further the polymer, which was then recovered after lyophilisation.

ALG_{ALD} – ^1H NMR (D_2O , 400 MHz, 25 $^{\circ}$ C), δ (ppm) 9.88 ($-\text{CHO}$, 1H, s), 8.44 (triazole, 1H, s), 8.00–7.66 (aromatic from



benzaldehyde, 4H, m), 7.47 (amide, 1H, m), 5.10–4.90 (alginate, 2H, m), 4.79 (H₂O), 4.25–3.50 (alginate, m), 3.50–2.75 (Alg-CO-NH-CH₂-CH₂-(O-CH₂-CH₂)₃-N-triazole) oligoethyl-ene glycol (PEG₃) (linker, m, 16H, m). ¹³C-(DMF, 120 MHz, 25 °C), δ (ppm)-195.4 (-CHO), 175.9 (-COOH-alginate), 175.4 (Alg-CONH-PEG₃-), 149.9 (-N-C=C-N=N-triazole ring), 149.8 (-C-CHO-aromatic ring), 135, 134, 133, 130, 129.6 (aromatic Cs from benzaldehyde), 129.5 (N-C=C-N=N-triazole ring), 100.9, 100.6, 100.1, 99.8, (Alginate-C-O-C), 80.0, 77.2, 76.1, 72.0 (Alginate-C-OH), 68.5, 67.5 (Alg-CO-NH-CH₂CH₂-O-(CH₂CH₂)₂-O-CH₂-CH₂-triazole), 67.0, 64.8, 62.4, 50.3, 46.6, 38.7 (Alg-CO-NH-CH₂-CH₂-(O-CH₂CH₂)₂-O-CH₂-CH₂-triazole-). IR (wavenumber, cm⁻¹) - 1600 (CONH amide carbonyl stretch), 1686 (-CHO carbonyl stretch), 2855 (aromatic CHO stretch), 2918 (triazole ring), 3062 (CH-alkane stretch from oligoethyl PEG₃ linker), 3278 (-COOH stretch).

ALG_{QSI} - ¹H NMR (D₂O/DMSO-d₆-90/10, 400 MHz, 70 °C), δ (ppm)-8.60–7.40 (aromatic and hydrazone protons of ACNQ-triazole conjugate, m), 5.30–5.00 (alginate, 2H, m), 4.75–4.00 (alginate, m), 4.71 (HDO), 4.20, 3.90 and 3.60–3.90 (Alg-CONH-CH₂-CH₂-(O-CH₂-CH₂)₃-triazole-, m), 2.50 (DMSO), 1.75–1.50 (m, -(CH₂)₉-CH₃ alkyl chain of ACNQ). ¹³C-(DMF, 120 MHz, 25 °C), δ (ppm) 161.0 (Alg-CONH-PEG₃-), 145.4 (-N-C=O-ACNQ drug), 140.1 (-N-C=C-N=N-triazole ring), 137.7 (C9-C(-N)-N=N-ACNQ drug), 134.0 (*tert*-aromatic unsubstituted Cs of ACNQ QSI chlorinated ring), 129.8–129.1 (C=C *tert*-aromatic), 127.3 (-N-NH=C-, hydrazone bond), 125.3 (aromatic C-Cl, ACNQ QSI drug), 121.2 (quart-C-N, aromatic-Cl ring ACNQ), 74.8, 71.8, 71.6, 70 (-C-O-C, alginate), 64.9–64.8 (-C-CO-, alginate), 54.1 (Alginate-C-OH), 48.3, 46.5 (Alg-CO-NH-CH₂CH₂-O-(CH₂CH₂)₂-O-CH₂-CH₂-triazole), 32.7–28.2–26.5 (Alg-CO-NH-CH₂-CH₂-(O-CH₂CH₂)₂-O-CH₂-CH₂-triazole-), 23.5 (CH₃-(CH₂)₇-CH₂-ACNQ QSI drug), 14.7 (CH₃-(CH₂)₇-CH₂-ACNQ), 9.2 (CH₃-(CH₂)₇-CH₂-ACNQ).

IR (wavenumber, cm⁻¹) 693, 713, 827 (C-Cl, heteroatom stretch from ACNQ), 1051, 1215 (C-N aliphatic stretch from ACNQ), 1510 (C=N hydrazone stretch), 2918 (triazole ring), 3060 (CH-alkane stretch from alkyl chain of ACNQ and oligoethyl PEG₃ linker), 3142 (aromatic stretch from ACNQ and aromatic linker), 3278 (-COOH stretch).

Fluorescein-labelled N₃-TEG-ALG. 6-Aminofluorescein (1 equiv.) was added to a stirred solution of CDMT (0.2 equiv.), NMM (1 equiv.) and N₃-PEG₃-ALG (1 equiv.) in H₂O/acetonitrile (3/2) mixture at 55 °C. The reaction mixture was allowed to stir overnight. Acetonitrile from the reaction mixture was removed by drying *in vacuo* followed by dilution of the product in DI water and dialysis against 10 K MWCO dialysis membrane for 2 days. The obtained solution was lyophilised and used without further purification.

Carboxyl-functional NPs from amino-functional polymer latex beads. Commercially available amino-functional latex polystyrene beads of diameter 50 or 200 nm (obtained from Sigma-Aldrich and ThermoFisher Scientific respectively) were suspended in water (2 mL) along with trimethylamine (15 μ L) and *N*-hydroxysulfosuccinimide sodium salt (20 mg). The resulting solution was left to stir at 0 °C for 1 hour followed by

addition of succinic anhydride (20 mg). The reaction mixture was allowed to stir overnight at room temperature before dialysis against a 2 kDa membrane to remove the excess of reagents. The diameter and zeta potentials of the obtained NPs were measured to confirm the successful functionalisation by succinic acid.

Determination of N₃ functional groups in N₃-TEG-ALG

The ERETIC method (Electronic Reference To access *In vivo* Concentrations)³⁸ was used in which 4 mg of N₃-TEG-ALG was dissolved in 600 μ L of D₂O to which 0.275 mg of hydroquinone dissolved in 100 μ L of D₂O was added. The peak of hydroquinone at 6.7 ppm (4H) was used to calculate the concentration of N₃-PEG₃ groups in the N₃-PEG₃-ALG polymer.

Protocol for nanoparticle (NP) formation

The NPs were prepared by a one-step *in situ* nanoprecipitation process. Briefly, the sodium alginate polymers (10 mg) were dissolved in PBS (10 mL) containing Tween 20 by sonication and added dropwise to a solution of CIP (10 mg) dissolved in 0.1 N HCl solution (0.1 mL). This solution was stirred overnight at RT. The solution obtained was dialysed against PBS for 72 hours to remove the free drug molecules. The dialysate was then freeze-dried and stored at 4 °C before use. The lyophilised NPs were equilibrated at room temperature and re-suspended in Tween 20 stabilised PBS (10 mL) before use. NPs without CIP were prepared by dissolving the 10 mg of polymer in 10 mL of 0.1 N HCl in buffer by sonication, followed by stirring overnight at RT.

Morphology, particle size, and zeta potential of NPs

The morphologies of the NPs were characterized by transmission electron microscopy (TEM; Tecnai G2, FEI, Oregon USA). The samples for TEM were prepared by adding dropwise the NP solution (1 mg mL⁻¹) onto the copper grid followed by drying for 4 hours before performing the microscopy. The particle sizes and zeta potentials of the NPs (1 mg mL⁻¹) were determined using a Zetasizer Nano ZS90, Malvern Instruments Ltd, UK.

Drug loading and pH-dependent release from the NPs

The amount of CIP in the NPs was quantified using a Cary 50 Bio UV spectrometer. Briefly, the amount of encapsulated CIP was obtained by dissolving different volumes of CIP-containing NPs in triplicate samples (1 μ L, 2 μ L, 3 μ L, 4 μ L, 5 μ L) in 0.1 N HCl solution (~1 mL) to release all the encapsulated CIP followed by dilution in PBS (total final volume-11 mL). The final concentration of CIP in the NPs was obtained (0.7 mg CIP per mL for ALG_{ALD}CIP and 0.8 mg CIP per mL for ALG_{QSI}CIP) by comparing the UV peak intensities with the calibration curve of CIP (λ_{max} = 275 nm). The amount of ACNQ in the NPs was estimated by directly correlating the complete consumption of azide groups in N₃-PEG₃-ALG (following 2100 cm⁻¹ peak corresponding to azide(N₃) by IR) to the concentration of added QSI-alkyne molecule after the click reaction. The amount of ACNQ drug was considered the same as



the amount of N_3 groups previously present in ALG-PEG₃-N₃ as determined by the ERETIC NMR technique.

For pH-responsive release, the release profiles of CIP ($\lambda_{\max} = 275$ nm) and ACNQ ($\lambda_{\max} = 240$ nm) from the NPs were studied using UV-VIS spectroscopy in pH 7.4 PBS buffer or pH 6.0 citric acid buffer. Typically, 2 mL of NPs solution (1.0 mg mL⁻¹) were placed in a dialysis bag (MWCO = 10 kDa), which was then immersed in 5 mL of release medium at different pH values at 37 °C and with constant shaking at 100 rpm. At the predetermined time points, 3 mL of medium was collected and replaced by 3 mL of fresh buffer.

Bacterial growth inhibition

To evaluate the growth inhibitory activity of alginate-CIP conjugates, free or encapsulated CIP was tested against *P. aeruginosa* PAO1-N cultures at concentrations 0.01, 0.05, 0.1, 0.2, 0.5 and 1 µg mL⁻¹. Bacteria were grown overnight in Luria broth (LB) at 37 °C. The next day the optical density (OD_{600 nm}) of the culture was adjusted to 0.01 in FAB³⁹ medium containing 10 mM glucose and 200 µL aliquots supplemented with CIP were loaded into the wells of a 96-well plate. As controls, medium only and wells containing NPs without ciprofloxacin were employed. Bacterial growth was monitored for 24 h at 37 °C in a 96-well plate TECAN Genios Pro spectrophotometer (Tecan, UK). The minimum inhibitory concentration (MIC) was defined as the antibiotic concentration where no visible bacterial growth was observed or OD_{600 nm} was <10% compared with the untreated control after 24 h of antibiotic exposure.

Biofilm viability and penetration assays

Mature pre-established PAO1-N biofilms were grown to assess the effects of co-delivered CIP and ACNQ on biofilm viability. For these assays, PAO1-N biofilms were grown on round glass coverslips (8 mm, #1.5 thickness) under flow conditions (20 rpm) in FAB containing 10 mM glucose medium inoculated with a diluted (OD_{600 nm} = 0.01) bacterial suspension from overnight cultures in LB. Biofilms were cultivated at 30 °C for 3 days with medium replacement every day. Biofilms were washed in PBS to remove loosely attached cells, and incubated for a further 24 h in fresh FAB medium supplemented with various treatments. These included free CIP and/or ACNQ as well as the NPs: ALG_{Ald} (empty NPs), ALG_{QSI}, ALG_{ALD}CIP and ALG_{QSI}CIP. With final concentrations of CIP and ACNQ of 60 µg mL⁻¹ (300× MIC) and 4 µg mL⁻¹ respectively. Biofilms exposed to each treatment were washed in PBS and the viabilities of the attached cells were evaluated using the LIVE/DEAD® BacLight™ Bacterial Viability kit (Molecular Probes, Life Technologies) according to the manufacturer's instructions. Following staining, coverslips were rinsed with sterile water and imaged using a LSM 700 laser scanning confocal microscope (CLSM) (Carl Zeiss, Germany). Viable and non-viable biomass quantification from image stacks of biofilms was done with Comstat2 software³⁹ (<http://www.comstat.dk>). Live/dead ratios were established for each treatment and com-

pared with untreated controls. Five independent assays were carried out in triplicate.

To ascertain that the reduced viability of the biofilms exposed to combined therapy was retained at different levels of exposure, a dose-response validation was carried out using different concentrations of CIP (5, 20 and 60 µg mL⁻¹ = 25×, 100× and 300× MIC respectively) while retaining the QSI concentration constant at 4 µg mL⁻¹. The biofilm viability was compared with that of free CIP treatment and an untreated control.

To evaluate NP diffusion through the biofilm matrix, ALG_{ALD} and ALG_{QSI} conjugates were labelled with fluorescein and tested against 3-day old PAO1-N biofilms. After 1, 2 and 24 h of incubation with NPs, biofilm samples were collected and stained with Syto64 fluorescent dye prior to CLSM image acquisition to simultaneously detect bacterial cells (red fluorescence) and NPs (green fluorescence). NP diffusion was determined by quantifying the fluorescein signal associated with each image stack and relating it to the biomass at different biofilm depths. Moreover, to relate biofilm penetration of alginate conjugates with other commercially available fluorescent NPs, the diffusion of blue fluorescent 50 nm polystyrene beads and red fluorescent 200 nm polystyrene beads carrying positive or negative zeta potentials were also tested in biofilms stained with Syto64 and Syto9 dyes respectively.

2D keratinocyte infection model

HaCat cells. Immortalised keratinocytes (HaCat) were used as a substrate for the 2D infection model. HaCat cells were expanded in T75 flasks (Corning), in RPMI-1460 medium supplemented with 10% heat inactivated fetal bovine serum (FBS), 2 mM L-glutamine and 1% penicillin (10 000 units)/streptomycin (10 mg mL⁻¹) until the monolayer was 80–85% confluent. Cells were trypsinised using trypsin/EDTA and seeded at 45 000 cells per cm² in an 8 well µ-slide Ibittreat chamber (Ibidi, Germany). When 90–100% confluent, cells were washed three times with Dulbecco's phosphate-buffered saline (DPBS). Prior to infection, HaCat cells were stained using CellTracker Green CMFDA (ThermoFisher), following the manufacturer's instructions.

Biofilm formation. An overnight culture of PAO1-N carrying the plasmid pME6032-*mCherry* in LB liquid medium supplemented with 125 µg mL⁻¹ of tetracycline was diluted 1 in 5 and incubated (37 °C, 200 rpm) until the OD_{600 nm} reached 0.8–1. After washing with PBS, the culture was normalised in RPMI-1460 supplemented with 10% FBS and 2 mM L-glutamine to an OD_{600 nm} = 0.01, further diluted 1 in 100 000 and 150 µL were added to each well containing confluent HaCat cells. ALG_{QSI} NPs containing 4 µg mL⁻¹ of QSI or ALG_{ALD} (empty NPs) were added at a final concentration 300 µg mL⁻¹. Infected cells were incubated at 37 °C, with 5% CO₂ and 95% humidity for 20 h prior to imaging using CLSM.

Image analysis. Biomass, average thickness and surface area of 8–10 image stacks of 20 h PAO1-N biofilms growing on HaCat cells monolayers were quantified using COMSTAT2 soft-



were employing automatic thresholding (Otsu's method) and without connected volume filtering.

3D skin infection model

Pig skin preparation and infection. Pig ears (obtained from an abattoir) were cleansed with sterile distilled water and depilated with a dry razor before soaking with antibacterial soap containing chlorhexidine gluconate 4.0% w/v (Hibiscrub, Boots) for 3 min. After removing the soap with sterile water, skin sections at the front and back of the ear were cut away from the subcutaneous cartilage. The sections were frozen at -20°C until required. A biopsy punch (7 mm) was used to remove skin plugs from freshly thawed skin samples. The skin plugs were immersed in ethanol for 20 min, then washed with PBS ($\times 2$) and immersed into $100\times$ Antibiotic Antimycotic solution for 10 minutes and washed with PBS ($\times 3$). The excess of water from skin plugs was removed with filter paper and the plugs were transferred to a 96-well plate containing 200 μL of soft agar. The skin was then infected with 10 μL of PAO1-N pME6032-*mCherry* suspension ($\text{OD}_{600\text{ nm}}$ 0.05) in PBS and incubated at 37°C , with 5% of CO_2 and 95% humidity for 24 h. 15 μL of CIP 1 mg mL^{-1} , ALG_{QSI} , $\text{ALG}_{\text{QSI}}\text{CIP}$ (containing 1 mg mL^{-1} of CIP), ALG_{ALD} or $\text{ALG}_{\text{ALD}}\text{CIP}$ (containing 1 mg mL^{-1} of CIP) were added to the infected skin plugs in triplicate and incubated for further 24 h.

Bacterial cell viable counts. Skin plugs were transferred to 1 mL of PBS and vortexed for 20 s to remove loosely attached bacteria. The samples were transferred for processing to FastPrep tubes containing 1 mL of PBS and six ceramic beads (2.8 mm) and were homogenised (FastPrep, MP Biomedicals), using the built-in 'skin' set-up. The supernatants were serially diluted 10-fold (10^{-1} to 10^{-8}) and each dilution plated in triplicate onto LB agar plates containing 125 $\mu\text{g mL}^{-1}$ of tetracycline. The plates were incubated at 37°C for 24 h.

Data analysis. GraphPad Prism 8 software was used for graphical representation and statistical analysis. Quantitative variables were compared using Student's *t* test. A *p*-value <0.05 was considered statistically significant.

Results and discussion

Polymer synthesis and characterisation

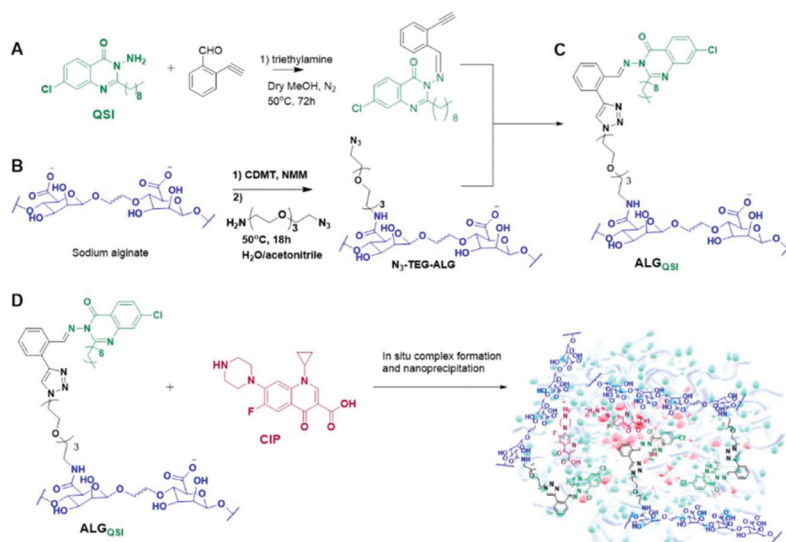
The design principles of the combination therapeutic were firstly that it needed to be derived from a simple, readily accessible polymer already used in human clinical applications. Secondly, the chemistries should enable a QSI to be attached *via* a pH-responsive linker and an antibiotic to be encapsulated. Finally, the whole system was required to self-assemble into lightly negatively-charged nanoparticles (NPs) in order to penetrate dense bacterial biofilms. Accordingly, we chose sodium alginates as the 'platform' material and modified the polymer with functionalities which enabled active agents to be incorporated *via* Schiff base linkages for *in situ* release in the acidic environment of a biofilm. We selected the QSI, 3-amino-7-chloro-2-nonylquinazolin-4(3*H*)-

one (ACNQ) (Ilangoan *et al.* 2013)^{31,40}, and utilised a triethyleneglycol spacer to append it to the alginate to ensure this hydrophobic drug was accessible to the aqueous environment when formulated. Finally, we opted for ciprofloxacin (CIP) as the antibiotic, as its positive charge at ambient pH values facilitated association with the alginate carboxylates and induced self-assembly of the system into NPs of sizes (150–200 nm) similar to those of *Pseudomonas* bacteriophages.³⁷ The synthetic scheme for the construction of the dual bioresponsive combination therapeutic nanoparticles is shown in Scheme 1.

The synthesis started with Schiff base formation between 2-ethynylbenzaldehyde and ACNQ to form (*Z*)-7-chloro-3-((2-ethynylbenzylidene)amino)-2-nonylquinazolin-4(3*H*)-one in $\sim 80\%$ yield. In parallel, CDMT/NMM based amide coupling was used to attach azide groups *via* a triethyleneglycol linker to the alginate backbone to obtain $\text{N}_3\text{-TEG-ALG}$ (Scheme 1). The derivatisation of the alginate backbone was confirmed by ^1H NMR and IR, with the presence of the azide groups apparent in FTIR spectra at 2100 cm^{-1} . The ERETIC method (Electronic REference To access *In vivo* Concentrations)³⁸ was used to estimate the amount of free azide groups in $\text{N}_3\text{-TEG-ALG}$ ($\sim 0.1\text{ }\mu\text{mol/1 mg}$). For the next steps, the well-established Cu-catalysed azide-alkyne click reactions were used to attach (*Z*)-7-chloro-3-((2-ethynylbenzylidene)amino)-2-nonylquinazolin-4(3*H*)-one with $\text{N}_3\text{-TEG-ALG}$ to obtain the key functional polymer ALG_{QSI} , (Scheme 1). We also prepared a second polymer, ALG_{ALD} , in which 2-ethynylbenzaldehyde was coupled to the $\text{N}_3\text{-TEG-ALG}$ backbone *via* the same click chemistry, but with no QSI attached. This was in order to render the polymer more amphiphilic, even without the QSI present, and thus potentially able to form nanoparticles with CIP in a manner analogous to that of ALG_{QSI} polymers.

For both the derivatised alginates (ALG_{ALD} and ALG_{QSI}), quantitative consumption of N_3 groups upon completion of the click reaction was confirmed by complete disappearance on 2100 cm^{-1} peak in IR. In addition, FTIR signals at 1686 cm^{-1} and 2855 cm^{-1} for aromatic aldehyde carbonyl stretching, 2918 cm^{-1} for triazole, along with triazole + amide + aromatic signals (7.2–8.5 ppm), $-\text{CHO}$ signal (10 ppm) in ^1H NMR, and characteristic peaks in ^{13}C NMR (for *e.g.* $-\text{CHO}$: 196 ppm) confirmed the successful formation of ALG_{ALD} . Similarly, for the ALG_{QSI} polymer, characteristic IR absorption bands corresponding to $\text{CH}=\text{NH}$ stretching for hydrazones (1510 cm^{-1}) and an intense band at 713 cm^{-1} for heteroatom C–Cl vibration confirmed the successful functionalisation with the QSI *via* a pH-responsive linkage. Characterisation of ALG_{QSI} *via* ^1H NMR was problematic at 25°C due to the tendency for the polymers to self-assemble, leading to poorly-resolving signals. However, using elevated temperature NMR at 70°C in a mixture of $\text{DMSO-}d_6 + \text{D}_2\text{O}$, the triazole + amide + aromatic signals in the range of 7.2–8.5 ppm, and ethylene glycol peaks (3.60–3.90 ppm) from $\text{N}_3\text{-TEG-NH}$ were apparent alongside the alginate peaks. The successful coupling of the QSI on the $\text{N}_3\text{-PEG}_3\text{-ALG}$ polymer was further verified by ^{13}C





Scheme 1 In (A) the QSI drug-3-amino-7-chloro-2-nonylquinazolin-4(3H)-one(ACNQ) was coupled with 2-ethynylbenzaldehyde to form the alkyne-functional intermediate (Z)-7-chloro-3-((2-ethynylbenzylidene)amino)-2-nonylquinazolin-4(3H)-one. In (B) carboxyl groups in sodium alginate were first activated then reacted with an α,ω -amine and azide-functional triethyleneglycol to form N_3 -TEG-ALG, which was then 'clicked' (as shown in C) with (Z)-7-chloro-3-((2-ethynylbenzylidene)amino)-2-nonylquinazolin-4(3H)-one to form the ALG_{QSI} polymer. In (D) Ciprofloxacin (CIP) was formulated into nanoparticles by an *in situ* nanoprecipitation process with ALG_{QSI} .

NMR, and the absence of signals corresponding to $-CHO$ in 1H , ^{13}C and FTIR for ALG_{QSI} also confirmed that the reversible hydrazone bond remained intact following synthesis and the conditions required for characterisation, with no evident liberation of ACNQ (Fig. 2).

Nanoparticle formulation and characterisation

After confirming the successful formation of the targeted amphiphilic structures- ALG_{ALD} and ALG_{QSI} , the next step was to prepare self-assembled nanostructures. This was readily accomplished by a single step nanoprecipitation in phosphate buffer, owing to the amphiphilic character of the hydrophobic (triazole + ACNQ C9 chain in ALG_{QSI}) and the hydrophilic (alginate and triethylene glycol) components. Both the polymers formed NPs with comparable diameters and zeta potentials (Table 1, Fig. 3A and B, Table S1, Fig. S11†). The negative zeta-potentials of the NPs with or without CIP confirmed that their outer exposed layer was predominantly the carboxyl-containing alginate chains.

The *in vitro* drug release profiles from the NPs were evaluated at pH 7.4 and 6.0 that were considered likely to be encountered in ambient biological conditions and in an established biofilm, respectively. Higher cumulative release of the QSI drug from ALG_{QSI} was observed at biofilm relevant pH 6.0 (0.5 M citrate buffer) than at pH 7.4 (0.1 M phosphate buffer), which was attributable to the accelerated hydrazone bond cleavage at the lower pH (Fig. 3C). Similarly, greater release of

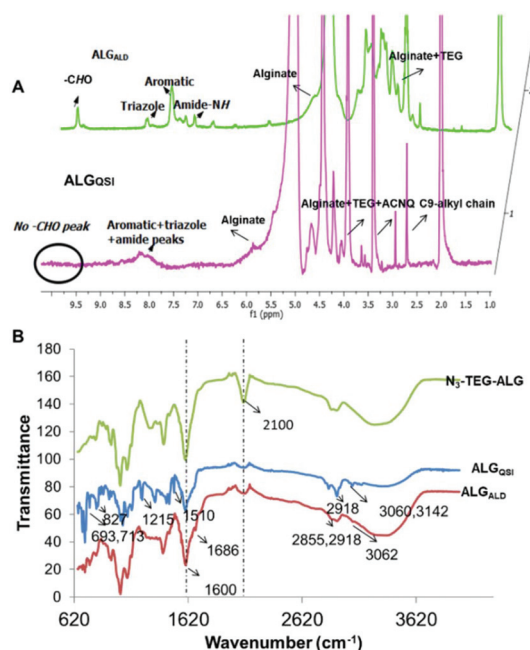


Fig. 2 (A) 1H NMR spectra of ALG_{QSI} at 70 °C and ALG_{ALD} at 25 °C. (B) FT-IR spectra comparing N_3 -PEG $_3$ -ALG, ALG_{QSI} and ALG_{ALD} showing complete consumption of azide (2100 cm^{-1}) for ALG_{QSI} and ALG_{ALD} , and other characteristic peaks.

Table 1 Properties of alginate-derived nanoparticles

Formulation	Diameter ^a /nm	Zeta potential/mV
ALG_{ALD}	221	−65.5
ALG_{QSI}	209	−39.7
$ALG_{ALD}CIP$	242	−42
$ALG_{QSI}CIP$	179	−44.8

^a Particle size reported is the diameter at the maximum peak height in the particle size distributions as obtained by dynamic light scattering.



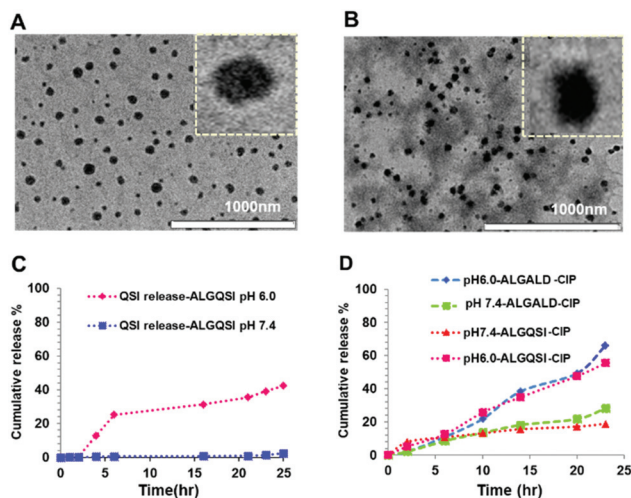


Fig. 3 TEM images of (A) ALGQSI-CIP and (B) ALGALD-CIP NPs. (C) Release profile over 24 h of ACNQ from ALGQSI at pH 6.0 and 7.4. (D) Ciprofloxacin release from ALGALD-CIP at pH 6.0 and 7.4.

ciprofloxacin from both ALG_{QSI} and ALG_{ALD} was observed at pH 6.0 than at pH 7.4 (Fig. 3D). This can be attributed to the high solubility of ciprofloxacin ($pK_{a \text{ acid}} = 6.16$) at this pH range overcoming its entrapment in the hydrophobic core along with the protonation of $-\text{COOH}$ in alginate, weakening the electrostatic interaction between CIP and alginate.

In vitro efficacy studies

The biofilm ECM is a major barrier to drug transport and efficacy in biofilm killing and removal. Our hypothesis was that alginate-based nanoparticles would be advantageous in overcoming this barrier and distributing throughout the

biofilm, especially as the net negative charges of the alginate-derivative NPs should prevent their accumulation at the biofilm surface. The latter problem limits the efficacy of many antimicrobial drugs, which are weakly basic and thus positively charged as they do not penetrate deeply into the biofilm core where antibiotic resistant or tolerant bacterial subpopulations are present.

Dye-labelled alginates were prepared by coupling 6-amino fluorescein to the previously synthesised N_3 -TEG-ALG and the polymers were formulated as before into ~ 200 nm nanoparticles. The NPs were administered to pre-established PAO1-N biofilms uniformly stained with SYTO64 (shown in blue in Fig. 4). No evident penetration by the fluorescent NPs was observed after 1 h incubation of the biofilms (fluorescein labelled NPs in yellow). However, after 2 h, the surface layers were partially covered with the NPs and within 24 h complete penetration throughout the biofilm was observed. In order to evaluate the role of alginate in determining the extent of biofilm penetration, we also tested commercially available fluorescent polystyrene NPs of comparable diameters (50 and 200 nm) with both +ve (commercially available) and -ve zeta potentials (derived by reaction of commercial $-\text{NH}_2$ terminated polystyrene NPs with succinic acid). These NPs irrespective of their zeta potentials or diameters (50 nm $+\text{53.7 mV}$ and $-\text{32.6 mV}$, 200 nm $+\text{48.4 mV}$ and $-\text{32.5 mV}$) were unable to penetrate even after 24 h and stayed mostly at the outer surfaces of the biofilm (Fig. 4, ESI Fig. S16†). These assays confirmed the ability of the modified alginate NPs to penetrate the PAO1-N biofilms effectively and to a much greater extent than non-alginate-based NPs.

To demonstrate the impact of combination therapy, we intended that ACNQ should act as a non-growth inhibitory adjuvant to CIP, by impacting on the biofilm architecture to render

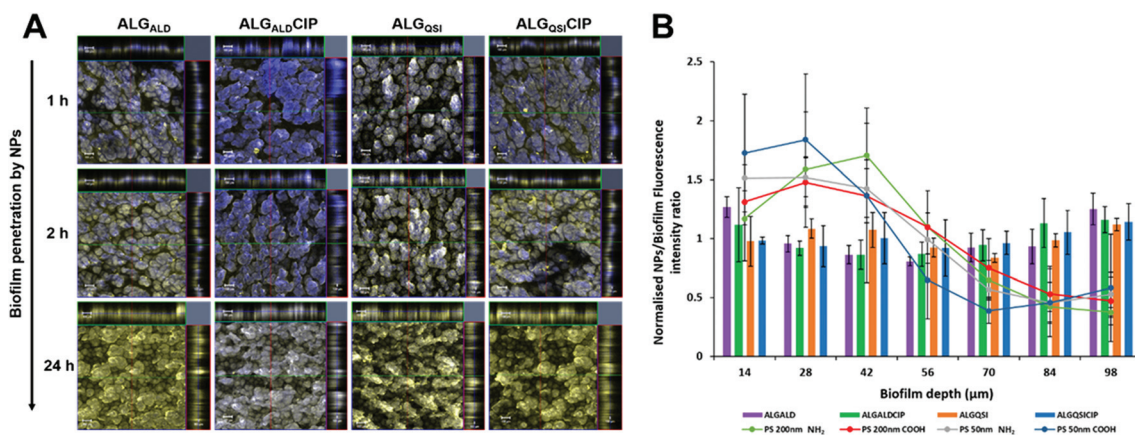


Fig. 4 Penetration of *P. aeruginosa* biofilms by alginate nanoparticles. In (A), confocal laser scanning microscopy (CLSM) images show penetration of 6-amino fluorescein-ALG_{ALD}, ALG_{ALD}-CIP, ALG_{QSI} and ALG_{QSI}-CIP NPs over time into PAO1-N biofilms stained with SYTO64 dye. The fluorescein labelled NPs are shown in yellow and the bacteria are stained blue. After incubating the biofilms for 1 h no penetration is observed as evident from the blue stained biofilm. The NPs begin to penetrate after 2 h of incubation as observed by the increase in yellow fluorescence from the biofilm structure. Within 24 h complete penetration to the biofilm bulk is observed, evident from the 3D Z-stack of the biofilm shown on the top and right of the main image. Scale bar: 100 μm. In (B), the penetration of the different ALG-based NPs within 24 h is quantified (bars), in contrast to the polystyrene (PS) NPs which are mostly present in the outer layer of the biofilm (28–42 μm depth, circles joined with lines). The fluorescence intensities of the ALG NPs and polystyrene NPs are normalised to the background fluorescence of the biofilm stain.



the biofilm sensitive to the killing action of the antibiotic. To validate this, we investigated the effects of ALG_{QSI} NPs on the growth of planktonic PAO1-N for 24 h. The presence of NPs inflicted no adverse effect on bacterial growth. Similarly, the biofilm viability also remained unaltered upon administration of ALG_{QSI} NPs over 24 h (ESI Fig. S13†). We also investigated whether the encapsulation of CIP in NPs could affect its activity by comparing the MICs of encapsulated and free CIP, which were demonstrated to be comparable ($0.2 \mu\text{g mL}^{-1}$) (ESI Fig. S12 and S13†). After confirming that the adjuvant was not affecting the growth or viability of PAO1-N in planktonic or biofilm states, we evaluated the effect of CIP on biofilm viability when co-delivered with ACNQ in the alginate NPs.

PAO1-N biofilms were established for 3 days before challenging with NP-delivered therapeutics (Fig. 5) followed by Live/Dead staining. Untreated biofilms (Fig. 5A), those treated with buffer (Fig. 5B) or ACNQ only (Fig. 5C) showed only live bacteria. When the biofilms were exposed to CIP, some evidence of dead bacteria was obtained due to areas of red staining within the biofilm (Fig. 5D) and treatment with the quorum sensing inhibitor ACNQ combined with CIP resulted in enhanced cell kill, but in 'patchy' domains (Fig. 5E). The most effective treatment was with ALG_{QSI}-CIP (Fig. 5F) in which deep penetration into the biofilm was apparent as evident from the large and diffuse red staining of dead bacteria.

Further quantification of the data is shown in Fig. 5G, including an additional formulation, ALG_{ALD}-CIP. These data showed that administration of CIP ($60 \mu\text{g mL}^{-1}$ – i.e. 300 times the MIC of planktonic PAO1-N) to biofilms resulted in ~50% cell kill after 24 h (Fig. 5G, red bar), and no noticeable improvement in the treatment of biofilm was observed by administering ACNQ in solution along with CIP (Fig. 5G,

brown bar). In both the cases, the 3D images of biofilms post treatment revealed that only the outer surfaces of the biofilms exposed to the drugs were affected whereas the bulk of the biofilms remained unaltered (ESI Fig. S15 and S16†). This is consistent with low penetration of both drugs through the biofilm. Moreover, the formation of precipitate was observed in the growth medium after around 4 h of ACNQ administration. This was due to the extremely hydrophobic nature of ACNQ making its delivery impractical without a carrier system. The limited efficacy of CIP alone in these assays, and the poor solubility of ACNQ thus suggested that a suitable delivery system might better penetrate the biofilm enabling more effective release of drugs *in situ*. However, despite evidence of biofilm penetration by the alginate-based NPs, a formulation of CIP with the ALG_{ALD} NPs did not cause any further reduction in biofilm viability (Fig. 5G purple bar). However, the combined formulation, i.e. ALG_{QSI}-CIP NPs containing both the antibiotic and ACNQ markedly reduced biofilm viability (Fig. 5F and G, orange bar). As evident from confocal microscopy, the bacterial viability was affected throughout the biofilm because of the deep penetration of alginate NPs and the likely delivery of both ACNQ and CIP in a spatio-temporally controlled manner. The viability of the biofilm was reduced to ~19% of the original value by ALG_{QSI}-CIP NPs compared to ~50% for ALG_{ALD}-CIP NPs applying the same dose of CIP ($60 \mu\text{g mL}^{-1}$). Furthermore, the combined effect of CIP and ACNQ was apparent over a wide concentration range for ALG_{QSI}-CIP NPs in terms of reduced biofilm viability, when compared with the corresponding concentrations of CIP alone ($5\text{--}60 \mu\text{g mL}^{-1}$) (ESI Fig. S14†). Therefore, the alginate NPs mediated effective penetration and delivered a QSI-induced increase in biofilm susceptibility to antibiotic.

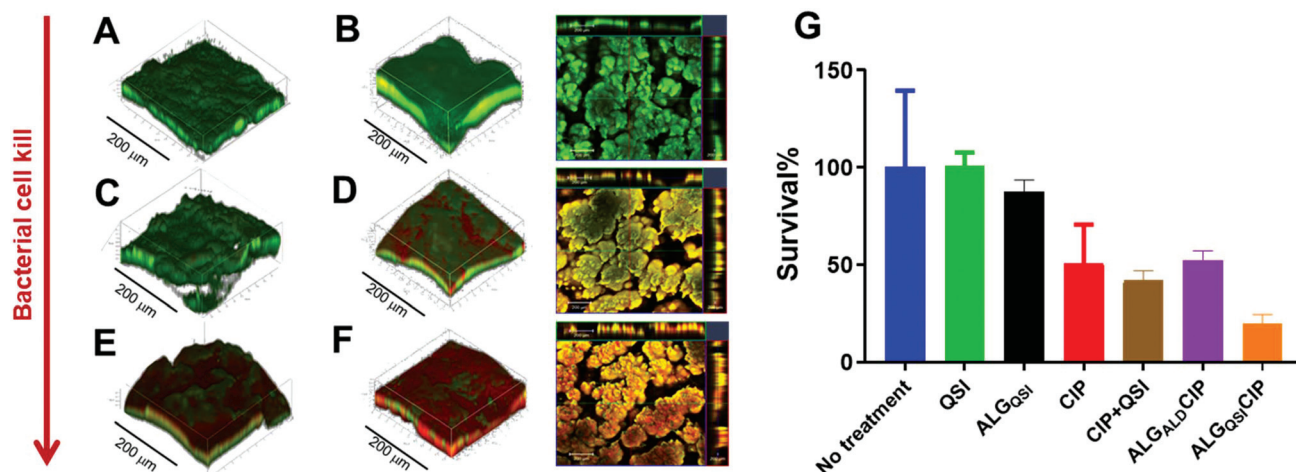


Fig. 5 Representative CLSM 3D Z-stack images PAO1-N biofilms after 3 days' growth and treatment for 24 hours with, (A) no drugs, (B) ALG_{QSI} NPs, (C) ACNQ ($4 \mu\text{g mL}^{-1}$) (D), CIP ($60 \mu\text{g mL}^{-1}$) (E) a combination of QSI ($4 \mu\text{g mL}^{-1}$) + CIP ($60 \mu\text{g mL}^{-1}$), and (F) ALG_{QSI}-CIP NPs with ACNQ(QSI)- $4 \mu\text{g mL}^{-1}$ and CIP- $60 \mu\text{g mL}^{-1}$. For images B, D and F, 2D microscopy images are included alongside the 3D CLSM, with overlapped live and dead imaged bacteria (depth profiles along the top and right borders). The live bacteria are depicted in green (SYTO9 dye) and the dead are shown in red colour (propidium iodide stain). In (G) are bar charts showing viability in PAO1-N biofilms quantified after treatment with different conditions for 24 hours. The concentrations of the drugs used were CIP- $60 \mu\text{g mL}^{-1}$, CIP ($60 \mu\text{g mL}^{-1}$) + ACNQ(QSI) ($4 \mu\text{g mL}^{-1}$), ALG_{ALD}-CIP (CIP- $60 \mu\text{g mL}^{-1}$) and ALG_{QSI}-CIP (ACNQ(QSI)- $4 \mu\text{g mL}^{-1}$ + CIP- $60 \mu\text{g mL}^{-1}$).



2D keratinocyte infection model

In addition to the effectiveness of the NP formulation in killing a preformed *P. aeruginosa* biofilm, its ability to prevent biofilm formation was also tested in a 2D keratinocyte skin epidermal cell infection model. Both the empty (ALG_{ALD}) and the NPs containing the QSI alone (ALG_{QSI}) were added at the time of bacterial inoculation and biofilm formation was assessed after 20 h. Fig. 6 shows that the presence of ALG_{QSI} significantly reduced biofilm formation (p -value <0.0001). However, it was apparent that the addition of the empty NPs alone also exerted a negative impact on biofilm formation (p -value <0.0001 for the 3 parameters) in this model. When comparing the impact of ALG_{QSI} and ALG_{AL} NPs on biofilm formation, bio-volume and average thickness but not surface area were significantly reduced in the presence of the QSI (p -values of 0.0105 and 0.0036 respectively; Fig. 6). Importantly, administration of ALG_{QSI} NPs protected the HaCat cells to a much greater extent than the untreated layer or those or treated with the ALG_{ALD} NPs (Fig. 6).

3D skin infection model

The efficacy of the NPs on a pre-existing *P. aeruginosa* skin infection was also tested. In this assay, *ex vivo* porcine skin plugs were inoculated with *P. aeruginosa* and after 24 h of infection, NPs were introduced and the skin incubated for a further 24 h. The viable bacterial loads recovered from the skin plugs were determined and the data are depicted in Fig. 7.

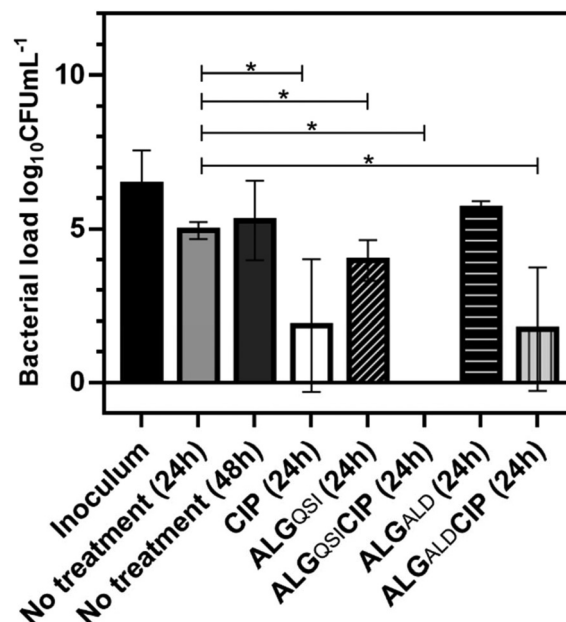


Fig. 7 Bacterial load (\log_{10} CFU mL⁻¹) recovered from skin infected with *P. aeruginosa* (PA) after 24 h or 48 h of incubation and/or after 24 h treatment with ciprofloxacin (CIP), ALG_{QSI}, ALG_{QSI}CIP, ALG_{ALD}, ALG_{ALD}CIP. The bacterial inoculum is also represented. *: Statistically significant (p -value < 0.05). The figure depicts the average of 4 experiments.

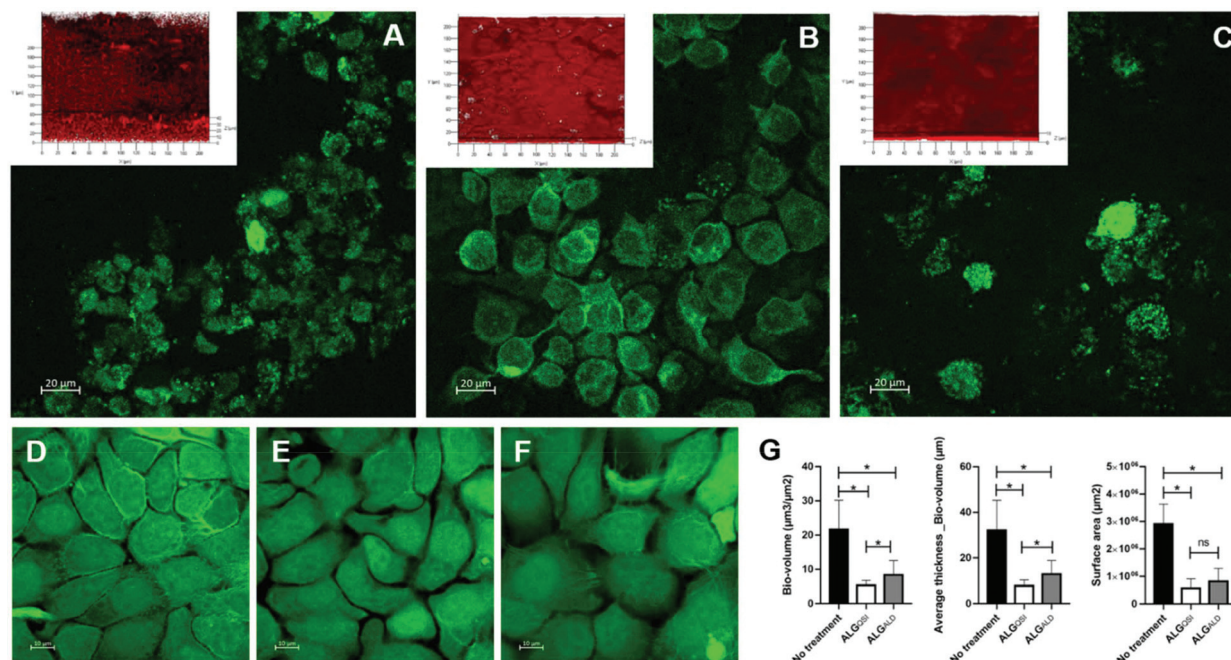


Fig. 6 2D Keratinocyte Infection Model. HaCat cell monolayer infected with PAO1-N for 20 h (A) and treated with ALG_{QSI} (B) or ALG_{ALD} (C) NPs (Image inserts show representative PAO1-N biofilms obtained). D, E & F: CLSM images of uninfected HaCat cells untreated (D), uninfected with 20 h ALG_{QSI} treatment (E) and uninfected with 20 h ALG_{ALD} treatment (F). In G, bar charts showing (L–R) the effects of the different treatments on PA biofilm volume, average thickness and surface area. *: Statistically significant (p -value <0.05). The figure represents the average of four repeats.



It is apparent from Fig. 7 that CIP alone (p -value <0.0001), ALG_{ALD}CIP (p -value <0.0001) and ALG_{QSI} (p -value = 0.0048) each significantly reduced the bacterial load. However, the combination of the QSI and CIP, when included in the alginate nanoparticle formulation, completely cleared the infection (p -value <0.0015).

These data together show that the combination NP therapeutic was the most effective against the microbial communities in both 2D and 3D assays and, most importantly, in a relevant *ex vivo* infected skin model. It is well established that bacterial-biofilm centred infections are recalcitrant, chronic and difficult to eradicate with conventional antibiotic therapy,⁸ and that new treatment modalities are urgently needed. *P. aeruginosa* biofilms are frequently associated with recurrent respiratory tract infections in cystic fibrosis and chronic obstructive pulmonary disease as well as diabetic wounds and implanted medical device (e.g. catheter) associated infections. Biofilms in general are highly tolerant to antibiotics and often require concentrations over 1000 times higher than those required to kill planktonic cells although newly formed biofilms are more susceptible than mature biofilms.⁸ Therefore, the need for more effective treatments capable of killing established biofilms is also paralleled by the requirement for methods to prevent biofilm formation. Here we have shown that alginate NPs are not only capable of penetrating and delivering an antimicrobial agent payload deep into a *P. aeruginosa* biofilm but are also, in the absence of a payload, able to reduce biofilm formation in an infection model where the biofilm is allowed to form on a keratinocyte skin cell monolayer. However, the inclusion of a biofilm disrupting QSI, not only reduced biofilm formation to a greater extent but also provided some protection for the keratinocytes. In a more sophisticated *ex vivo* porcine skin model, the incorporation of both an antibiotic and a QSI within the alginate NP delivery system was required to eradicate completely the viable bacteria. As observed for the pre-formed biofilm, the dual action NP delivery system was far more effective than ciprofloxacin in solution, suggesting a clear advantage of incorporating the antibiotic in a carrier. In addition, the combined delivery system effectively killed the biofilm *in situ* with little apparent dispersal of the biofilm bacteria. This may offer an additional advantage in clinical practice, in that it reduces the likelihood of bacterial aggregates breaking away to initiate biofilm formation at new sites. Furthermore, while the QSI ACNQ has previously been shown to inhibit biofilm formation,⁴⁰ its effect on preformed biofilms when delivered in NPs had not been shown before. Although ACNQ has a micromolar IC₅₀, more potent PqsR analogues with nanomolar efficacies have recently been described and may offer improved potency as antibiotic adjuvants when delivered in NPs.^{23,41} Alternatively, a more rapid route to clinical testing could be achieved by incorporating re-purposed FDA-approved drugs such as clofoctol, an compound that acts as an antibiotic against Gram-positive but not Gram-negative bacteria but is a potent PqsR antagonist for *P. aeruginosa*.⁴²

For the delivery system we selected alginate as the carrier polymer, in part because alginate oligomers have previously

been shown to inhibit biofilm formation and potentiate the action of antibiotics against *P. aeruginosa*.^{33,43} However, *P. aeruginosa* strains produce heterogeneous ECMs that may contain one or more of three different exopolysaccharides including alginate.⁴⁴ The *P. aeruginosa* strain PAO1-N used in our assays do not produce alginate containing biofilms and therefore it would be of interest to determine the efficacy of the NP delivery system in future against the mucoid-alginate producing *P. aeruginosa* strains that are frequently found in the lungs of individuals with cystic fibrosis who are chronically colonized by *P. aeruginosa*.^{43,44} In addition, further work will be required to determine whether dual action NPs are capable of eradicating *P. aeruginosa* biofilms in murine infection models and can be formulated for the treatment and prevention and treatment of chronic wounds and medical device associated infections. The advantages of a nanoparticulate formulation in this setting are the ability to incorporate multiple agents which could in principle be released by a range of *in situ* disease-related triggers, such as inflammatory oxidative stress⁴⁵ in addition to local pH, thus enabling tuning of therapy to particular wound conditions. Finally, it would be of interest to evaluate the effects of functionality, charge, polymer/nanoparticle size and architecture systematically in bacterial recognition, biofilm penetration and therapeutic delivery.^{46–49} It is well-established that natural nanoparticulates such as viruses can penetrate through many biological barriers, and biomimicry of bacteriophage structural features might in future allow development of highly active synthetic NPs which exhibit functional mimicry and anti-bacterial action also.

Conclusions

In this study we have shown that alginate biopolymers can be modified to contain a responsive linker to the QSI ACNQ, and induced to self-assemble in the presence of an antibiotic, ciprofloxacin, to generate well-defined nanoparticles. These materials were able to release both the encapsulated antibiotic and the conjugated QSI in response to pH values expected in bacterial biofilms. When evaluated for efficacy against *P. aeruginosa* biofilms the nanoparticles were more effective in bacterial killing than the antibiotic alone, and the extent of cell killing was retained deep into the biofilm layer. The most significant data related to the activity of the nanoparticles in 2D keratinocyte and 3D *ex vivo* skin infection models. The alginate NPs showed some protective activity against *P. aeruginosa* infection in keratinocytes even in the absence of antibiotic, but the full combination therapeutic system completely cleared the infection in the 3D *ex vivo* skin model. In summary, the results demonstrate considerable promise for nanoparticle combination therapeutics, in the prevention of biofilm formation, in the reduction in biofilm load and through enhanced cell killing in established biofilms of the important ESKAPE pathogen *P. aeruginosa*.



Data access statement

All raw data created during this research are openly available from the corresponding author (cameron.alexander@nottingham.ac.uk) and at the University of Nottingham Research Data Management Repository (<https://rdmc.nottingham.ac.uk/>) and all analysed data supporting this study are provided in the ESI† accompanying this paper.

Conflicts of interest

There are no conflicts to declare.

Funding sources

This work was supported by the Engineering and Physical Sciences Research Council [grant numbers EP/N006615/1 and EP/K005138/1, EP/N03371X/1]; the Biotechnology and Biological Sciences Research Council (BBSRC) [grant number BB/R012415/1] and the Royal Society [Wolfson Research Merit Award WM150086] (to CA). This project has received funding from the EMPIR programme co-financed by the Participating States and from the European Union's Horizon 2020 research and innovation programme [grant reference 15HLT01 MetVBadBugs]

Acknowledgements

We thank the Nanoscale and Microscale Research Centre and the School of Life Sciences Imaging Facility (SLIM) at the University of Nottingham for providing access to advanced light and scanning microscopy instrumentation, and Drs Emily Smith and Tim Self at the University of Nottingham for valuable guidance. We also thank Christine Grainger-Boulty, Esme Ireson and Paul Cooling for skilled technical assistance, Alex Truman for ACNQ synthesis and Dr Sian Rankin-Turner, Elizabeth Hufton and Carol Turrill for invaluable project support.

Notes and references

- B. D. Brooks and A. E. Brooks, *Adv. Drug Delivery Rev.*, 2014, **78**, 14–27.
- M. Lakemeyer, W. N. Zhao, F. A. Mandl, P. Hammann and S. A. Sieber, *Angew. Chem., Int. Ed.*, 2018, **57**, 14440–14475.
- P. Speck, *Nature*, 2013, **496**, 169.
- S. R. Partridge, S. M. Kwong, N. Firth and S. O. Jensen, *Clin. Microbiol. Rev.*, 2018, **31**(4), e00088-17.
- S. Mukherjee and B. L. Bassler, *Nat. Rev. Microbiol.*, 2019, **17**, 371–382.
- H. Koo, R. N. Allan, R. P. Howlin, P. Stoodley and L. Hall-Stoodley, *Nat. Rev. Microbiol.*, 2017, **15**, 740–755.
- R. M. Donlan and J. W. Costerton, *Clin. Microbiol. Rev.*, 2002, **15**, 167–193.
- O. Ciofu and T. Tolker-Nielsen, *Front. Microbiol.*, 2019, **10**, 913.
- L. Hall-Stoodley, J. W. Costerton and P. Stoodley, *Nat. Rev. Microbiol.*, 2004, **2**, 95–108.
- T. Parandhaman and S. K. Das, *Biomater. Sci.*, 2018, **6**, 3356–3372.
- N. Perez-Soto, L. Moule, D. N. Crisan, I. Insua, L. M. Taylor-Smith, K. Voelz, F. Fernandez-Trillo and A. M. Krachler, *Chem. Sci.*, 2017, **8**, 5291–5298.
- N. Doroshenko, S. Rimmer, R. Hoskins, P. Garg, T. Swift, H. L. M. Spencer, R. M. Lord, M. Katsikogianni, D. Pownall, S. MacNeil, C. W. I. Douglas and J. Shepherd, *Biomater. Sci.*, 2018, **6**, 2101–2109.
- L. T. Liu, B. Ercan, L. L. Sun, K. S. Ziemer and T. J. Webster, *ACS Biomater. Sci. Eng.*, 2016, **2**, 122–130.
- C. F. Garcia, F. Stangl, A. Gotz, W. N. Zhao, S. A. Sieber, M. Opitz and O. Lieleg, *Biomater. Sci.*, 2019, **7**, 220–232.
- J. X. Guo, Y. Liu, Y. L. Chen, J. Q. Li and H. X. Ju, *Chem. Sci.*, 2018, **9**, 5906–5911.
- I. Di Bonaventura, X. Jin, R. Visini, D. Probst, S. Javor, B. H. Gan, G. Michaud, A. Natalello, S. M. Doglia, T. Kohler, C. van Delden, A. Stocker, T. Darbre and J. L. Reymond, *Chem. Sci.*, 2017, **8**, 6784–6798.
- B. Wang, Z. Ye, Q. Xu, H. Liu, Q. Lin, H. Chen and K. Nan, *Biomater. Sci.*, 2016, **4**, 1731–1741.
- J. S. Dickschat, *Nat. Prod. Rep.*, 2010, **27**, 343–369.
- K. Reuter, A. Steinbach and V. Helms, *Perspect. Med. Chem.*, 2016, **8**, 1–15.
- P. Williams, K. Winzer, W. C. Chan and M. Camara, *Philos. Trans. R. Soc., B*, 2007, **362**, 1119–1134.
- B. Rémy, S. Mion, L. Plener, M. Elias, E. Chabrière and D. Daudé, *Front. Pharmacol.*, 2018, **9**, 203–203.
- P. Williams, *Emerging Top. Life Sci.*, 2017, **1**, 23–30.
- F. Soukarieh, P. Williams, M. J. Stocks and M. Cámara, *J. Med. Chem.*, 2018, **61**, 10385–10402.
- M. J. Kratochvil, Y. Tal-Gan, T. Yang, H. E. Blackwell and D. M. Lynn, *ACS Biomater. Sci. Eng.*, 2015, **1**, 1039–1049.
- E. Cavaleiro, A. S. Duarte, A. C. Esteves, A. Correia, M. J. Whitcombe, E. V. Piletska, S. A. Piletsky and I. Chianella, *Macromol. Biosci.*, 2015, **15**, 647–656.
- E. V. Piletska, G. Stavroulakis, L. D. Larcombe, M. J. Whitcombe, A. Sharma, S. Primrose, G. K. Robinson and S. A. Piletsky, *Biomacromolecules*, 2011, **12**, 1067–1071.
- J. K. Vasquez and H. E. Blackwell, *ACS Infect. Dis.*, 2019, **5**, 484–492.
- M. E. Boursier, J. B. Combs and H. E. Blackwell, *ACS Chem. Biol.*, 2019, **14**, 186–191.
- A. G. Palmer, A. C. Senechal, T. C. Haire, N. P. Mehta, S. D. Valiquette and H. E. Blackwell, *ACS Chem. Biol.*, 2018, **13**, 3115–3122.
- J. N. Pendleton, S. P. Gorman and B. F. Gilmore, *Expert Rev. Anti-Infect. Ther.*, 2013, **11**, 297–308.
- A. Ilangoan, M. Fletcher, G. Rampioni, C. Pustelny, K. Rumbaugh, S. Heeb, M. Camara, A. Truman, S. R. Chhabra, J. Emsley and P. Williams, *PLoS Pathog.*, 2013, **9**(7), e1003508.



- 32 T. F. Mah, B. Pitts, B. Pellock, G. C. Walker, P. S. Stewart and G. A. O'toole, *Nature*, 2003, **426**, 306–310.
- 33 S. Khan, A. Tondervik, H. Sletta, G. Klinkenberg, C. Emanuel, E. Onsoyen, R. Myrvold, R. A. Howe, T. R. Walsh, K. E. Hill and D. W. Thomas, *Antimicrob. Agents Chemother.*, 2012, **56**, 5134–5141.
- 34 C. Berne, A. Ducret, G. G. Hardy and Y. V. Brun, *Microbiol. Spectrum*, 2015, **3**(4), MB-0018-2015.
- 35 J. Shephard, A. J. McQuillan and P. J. Bremer, *Appl. Environ. Microbiol.*, 2008, **74**, 6980–6986.
- 36 S. M. Morgan, A. Alshamkhani, D. Callant, E. Schacht, J. F. Woodley and R. Duncan, *Int. J. Pharm.*, 1995, **122**, 121–128.
- 37 X. Cui, J. You, L. Sun, X. Yang, T. Zhang, K. Huang, X. Pan, F. Zhang, Y. He and H. Yang, *Sci. Rep.*, 2016, **6**, 39130.
- 38 S. Akoka, L. Barantin and M. Trierweiler, *Anal. Chem.*, 1999, **71**, 2554–2557.
- 39 A. Heydorn, A. T. Nielsen, M. Hentzer, C. Sternberg, M. Givskov, B. K. Ersboll and S. Molin, *Microbiology*, 2000, **146**(Pt 10), 2395–2407.
- 40 A. Ilangovan, M. Fletcher, G. Rampioni, C. Pustelny, K. Rumbaugh, S. Heeb, M. Cámara, A. Truman, S. R. Chhabra, J. Emsley and P. Williams, *PLoS Pathog.*, 2013, **9**, e1003508.
- 41 F. Soukarieh, E. Vico Oton, J. F. Dubern, J. Gomes, N. Halliday, M. de Pilar Crespo, J. Ramirez-Prada, B. Insuasty, R. Abonia, J. Quiroga, S. Heeb, P. Williams, M. J. Stocks and M. Camara, *Molecules*, 2018, **23**, 257.
- 42 F. D'Angelo, V. Baldelli, N. Halliday, P. Pantalone, F. Polticelli, E. Fiscarelli, P. Williams, P. Visca, L. Leoni and G. Rampioni, *Antimicrob. Agents Chemother.*, 2018, **62**(11), e01296-18.
- 43 L. C. Powell, M. F. Pritchard, E. L. Ferguson, K. A. Powell, S. U. Patel, P. D. Rye, S.-M. Sakellakou, N. J. Buurma, C. D. Brilliant, J. M. Copping, G. E. Menzies, P. D. Lewis, K. E. Hill and D. W. Thomas, *npj Biofilms Microbiomes*, 2018, **4**, 13.
- 44 D. J. Wozniak, T. J. Wyckoff, M. Starkey, R. Keyser, P. Azadi, G. A. O'Toole and M. R. Parsek, *Proc. Natl. Acad. Sci. U. S. A.*, 2003, **100**, 7907–7912.
- 45 G. Saravanakumar, J. Kim and W. J. Kim, *Adv. Sci.*, 2017, **4**, 1600124.
- 46 E. Leire, S. P. Amaral, I. Louzao, K. Winzer, C. Alexander, E. Fernandez-Megia and F. Fernandez-Trillo, *Biomater. Sci.*, 2016, **4**, 998–1006.
- 47 N. Perez-Soto, O. Creese, F. Fernandez-Trillo and A. M. Krachler, *ACS Chem. Biol.*, 2018, **13**, 3021–3029.
- 48 E. P. Magennis, F. Fernandez-Trillo, C. Sui, S. G. Spain, D. J. Bradshaw, D. Churchley, G. Mantovani, K. Winzer and C. Alexander, *Nat. Mater.*, 2014, **13**, 748–755.
- 49 L. T. Lui, X. Xue, C. Sui, A. Brown, D. I. Pritchard, N. Halliday, K. Winzer, S. M. Howdle, F. Fernández Trillo, N. Krasnogor and C. Alexander, *Nat. Chem.*, 2013, **5**, 1058–1065.

